

Impact of Cavity on Molecular Ionization Spectra

Csaba Fábri,^{1, 2, a)} Gábor J. Halász,³ Lorenz S. Cederbaum,⁴ and Ágnes Vibók^{2, 5, b)}

¹⁾*HUN-REN-ELTE Complex Chemical Systems Research Group,
H-1518 Budapest 112, Hungary*

²⁾*Department of Theoretical Physics, University of Debrecen, P.O. Box 400,
H-4002 Debrecen, Hungary*

³⁾*Department of Information Technology, University of Debrecen, P.O. Box 400,
H-4002 Debrecen, Hungary*

⁴⁾*Theoretische Chemie, Physikalisch-Chemisches Institut, Universität Heidelberg,
D-69120, Germany*

⁵⁾*ELI-ALPS, ELI-HU Non-Profit Ltd, H-6720 Szeged, Dugonics tér 13,
Hungary*

Ionization phenomena are widely studied for decades. With the advent of cavity technology, the question arises how quantum light affects molecular ionization. As the ionization spectrum is recorded from the neutral ground state, it is usually possible to choose cavities which exert negligible effect on the neutral ground state, but have significant impact on the ion and the ionization spectrum. Particularly interesting are cases where the ion exhibits conical intersections between close-lying electronic states, which gives rise to substantial nonadiabatic effects. Assuming single-molecule strong coupling, we demonstrate that vibrational modes irrelevant in the absence of cavity play a decisive role when the molecule is in the cavity. Here, dynamical symmetry breaking is responsible for the ion-cavity coupling and high symmetry enables control of the coupling via molecular orientation relative to the cavity field polarization. Significant impact on the spectrum by the cavity is found and shown to even substantially increase for less symmetric molecules.

^{a)}Electronic mail: ficsaba@staff.elte.hu

^{b)}Electronic mail: vibok@phys.unideb.hu

Molecular cavity quantum electrodynamics studies the interaction of confined electromagnetic field modes with molecules. Photon-molecule coupling gives rise to mixed light-matter states which are called polaritons carrying both photonic and molecular features. Since the pioneering experimental work of the Ebbesen group reported in 2012,¹ "polaritonic chemistry" has become a rapidly emerging field of physics and chemistry opening up novel possibilities to manipulate material properties. An array of intriguing experimental and theoretical works have demonstrated that polaritonic states can dramatically alter physical and chemical properties of molecular systems.²⁻⁵³ Strong coupling has been shown to influence chemical reactivity by enhancing or suppressing available mechanisms^{1,54}, and mediating new ones.¹⁶ Strong coupling can also enhance charge and energy transfer,²⁶ modify absorption spectra^{9,20,28,55} and give rise to strong nonadiabatic effects in molecules^{6,7,9,12,20-22,25,28,31,37,38,40,56} by providing ultrafast nonradiative decay channels.^{11,13,15,57}

Coupling between nuclear and electronic motions in polyatomic molecules induces nonadiabatic phenomena, such as conical intersections (CIs).⁵⁸⁻⁶³ CIs between electronic potential energy surfaces (PESs) result in remarkable changes in the dynamical, spectroscopic and topological properties of molecules. Additionally, nonadiabatic effects can also be created by external classical or quantized electromagnetic fields.^{4,6,9,28,64,65} In such cases, the laser field or a confined mode of the cavity can couple molecular electronic states and light-induced CIs (LICIs) are formed. Nonadiabatic effects associated with LICIs are essentially identical to natural ones.

We investigate the combined impact of natural and light-induced CIs on the ionization spectrum of a molecule in a cavity. Although natural and light-induced nonadiabatic phenomena^{6,7,12,13,15,17,21,22,25,37,38,54,56,57,66} and their signatures in absorption spectra^{9,20,28,31,55} have been examined in neutral molecules placed into a cavity, the ionization of molecules inside a cavity has remained largely unexplored (Refs. 67 and 68 investigated the ionization potential of molecules in cavity). To fill this gap, we choose the butatriene (BT, C_4H_4) molecule as a showcase system. Since the low-energy (cavity-free) ionization spectrum of BT already exhibits a dramatic fingerprint of a natural CI,^{69,70} BT is a compelling candidate for the current study. In particular, a natural CI is formed between the electronic ground

(X $^2B_{2g}$) and first excited states (A $^2B_{2u}$) of the BT cation (BT⁺). The CI is located near the Franck–Condon (FC) region of the neutral BT ground state and gives rise to an unexpected and well-separated band (“mystery band”) in the ionization spectrum.⁷¹ The origin of the mystery band was clarified in Ref. 69 where it was also concluded that a vibronic coupling model treating two vibrational modes is capable of accurately reproducing the low-energy experimental ionization spectrum. Later, an all-mode vibronic coupling model was developed and gave results essentially identical to the 2-mode model.⁷⁰

Coupling to cavity leads to LICI formation and the ionization spectrum is shaped by the joint effect of natural and light-induced CIs. In sharp contrast to natural CIs, the position of the LICI and the light-induced nonadiabatic coupling strength can be controlled by the cavity frequency and coupling strength, respectively. This allows for a systematic control of light-induced nonadiabaticity including the competition between natural and light-induced CIs. The scenario of the current work is outlined as follows. BT is ionized with a weak laser pulse in a low-frequency cavity. In neutral BT the ground and first excited electronic states are well separated energetically (~ 5.7 eV at the FC point). Therefore, a low-frequency cavity mode tailored to bring the ground and first excited states of BT⁺ into resonance does not couple the neutral BT ground state to other states. However, resonant coupling of the X and A states of BT⁺ leads to the formation of LICIs. Consequently, significant cavity-induced changes in the ionization spectrum, also affecting the mystery band, are expected compared to the cavity-free case. We shall see that BT is particularly interesting for studying nonadiabatic effects. Due to symmetry, the cavity does not couple to BT⁺ at the FC point. All couplings are induced dynamically by symmetry-breaking vibrational modes. Symmetry also allows to control which kind of modes couple.

A single molecule coupled to a lossless cavity mode is described by the Hamiltonian⁷²

$$\hat{H}_{\text{cm}} = \hat{H}_0 + \hbar\omega_{\text{cav}}\hat{a}^\dagger\hat{a} - g\hat{\mu}\vec{e}(\hat{a}^\dagger + \hat{a}) \quad (1)$$

where \hat{H}_0 is the molecular Hamiltonian, ω_{cav} denotes the cavity angular frequency, \hat{a}^\dagger and \hat{a} are creation and annihilation operators, g refers to the coupling strength parameter, $\hat{\mu}$ corresponds to the molecular electric dipole moment and \vec{e} is the field polarization vector. In this work, we treat a molecule coupled to a plasmonic cavity mode and omit the dipole

self-energy (DSE) term (see Refs. 46, 73 and 74 for further explanation). It is worth noting that strong coupling has been achieved experimentally at the single-molecule (emitter) level in plasmonic cavities.^{3,47} The relevance of the DSE, including its role in collective vibrational strong coupling, has been investigated thoroughly.^{51,75} It was also concluded that without the DSE the coupled cavity-molecule system does not have a ground state.⁷⁵ We stress that in the current computational model a stable ground state was found without the DSE term. Inclusion of the DSE would also modify our symmetry arguments, for example, the DSE term would give a nonzero contribution at the FC point. Moreover, it is important to note that plasmonic cavity modes have a short lifetime.⁴⁶ However, in the current case the finite lifetime of the cavity mode primarily influences the shape of the spectral lines (i.e., the spectral lines would have a certain width) in the ionization spectrum. Since we are interested in identifying cavity-induced effects on line positions and intensities, cavity loss has been omitted from our computational protocol in this first investigation of the subject.

Considering two electronic states (X and A) of BT^+ , the Hamiltonian of Eq. (1) reads

$$\hat{H}_{\text{cm}} = \begin{bmatrix} \hat{T} + V_X & V_{XA} & W_X^{(1)} & W_{XA}^{(1)} & \dots \\ V_{XA} & \hat{T} + V_A & W_{XA}^{(1)} & W_A^{(1)} & \dots \\ W_X^{(1)} & W_{XA}^{(1)} & \hat{T} + V_X + \hbar\omega_{\text{cav}} & V_{XA} & \dots \\ W_{XA}^{(1)} & W_A^{(1)} & V_{XA} & \hat{T} + V_A + \hbar\omega_{\text{cav}} & \dots \\ \vdots & \vdots & \vdots & \vdots & \ddots \end{bmatrix} \quad (2)$$

where \hat{T} is the kinetic energy operator, V_X and V_A are the ground-state and excited-state PESs, and V_{XA} describes the vibronic coupling between X and A in the diabatic representation. The cavity-molecule coupling is characterized by $W_\alpha^{(n)} = -g\sqrt{n}\mu_\alpha$ with $\alpha = X, A$ and $W_{XA}^{(n)} = -g\sqrt{n}\mu_{XA}$ ($n = 0, 1, 2, \dots$ labels Fock states of the cavity mode). In practical computations we have included all counter-rotating terms and employed the maximal photon numbers $n_{\text{max}} = 15$ (for polarizations $\mathbf{e} = (1, 0, 0)$ and $\mathbf{e} = (0, 1, 0)$) and $n_{\text{max}} = 20$ (for $\mathbf{e} = (1, 1, 0)/\sqrt{2}$). The permanent (PDM) and transition (TDM) dipole moment components along \vec{e} are denoted by μ_α ($\alpha = X, A$) and μ_{XA} , respectively. We stress that the rotational degrees of freedom are omitted in the current work and the orientation of the molecule is kept fixed with respect to \vec{e} . Polaritonic (adiabatic) PESs can be obtained by diagonalizing

the potential energy part of \hat{H}_{cm} .

Vibronic coupling models have been extremely successful in describing ionization spectra.^{58,76} Accordingly, the potentials V_X , V_A and V_{XA} , and also the terms $W_X^{(n)}$, $W_A^{(n)}$ and $W_{XA}^{(n)}$, are expanded around the FC point of D_{2h} point-group symmetry. In the 2-mode vibronic coupling model of BT^+ ,^{58,69,70} the two electronic states are coupled by the torsional mode of A_u symmetry (coupling mode) and the energy gap between them is tuned by the central C-C stretch mode of A_g symmetry (tuning mode). Vibrational modes relevant for the current study are listed in Table II of the Supporting Information and see Fig. 1 there for body-fixed axis definitions. The coupling (ν_c) and tuning (ν_t) modes correspond to ν_5 and ν_{14} , respectively. Following earlier work,^{69,70} the potentials are approximated as

$$\begin{aligned} V_\alpha &= \epsilon_\alpha + \frac{1}{2}\omega_t^2 Q_t^2 + \frac{1}{2}\omega_c^2 Q_c^2 + \kappa_\alpha Q_t \\ V_{XA} &= \lambda Q_c \end{aligned} \quad (3)$$

where $\alpha = X, A$, Q_t and Q_c denote normal coordinates of the tuning and coupling modes, respectively, while ω_t and ω_c refer to ground-state vibrational frequencies of BT. For a more detailed description of the 2-mode model and parameter values we refer to Sections II and IV/A of the Supporting Information.

Group-theoretical considerations (see Section I of the Supporting Information) reveal that the TDM and PDMs all vanish at the FC point. Moreover, the TDM and PDMs remain zero upon moving away from the FC point along ν_c and ν_t . In other words, the cavity does not couple to BT^+ in the 2-mode model and in order to enable this coupling we incorporate two additional modes, one which produces TDM (ν_9) and one which produces PDMs (ν_{10}) upon displacement from the FC point, breaking the D_{2h} symmetry. We shall denote these modes by ν_{TDM} and ν_{PDM} and address the resulting model consisting of these modes necessary to couple the cavity and the molecule and the tuning and coupling modes necessary to describe the natural CI, as the 4-mode model. Obviously, the choice of ν_{TDM} and ν_{PDM} is not unique. In the current work, modes ν_{TDM} and ν_{PDM} were selected to generate appreciable TDM and PDM values along two orthogonal axes (see the discussion later). The PDM and TDM functions are expressed as $\mu_\alpha = \beta_\alpha Q_{\text{PDM}}$ and $\mu_{XA} = \gamma Q_{\text{TDM}}$, respectively, where $\alpha = X, A$, and Q_{PDM} and Q_{TDM} are normal coordinates of the PDM and TDM modes. Values of the

parameters β_α and γ as well as further information on the construction of the PDM and TDM functions can be found in Sections IV/A and IV/B of the Supporting Information. For the evaluation of Hamiltonian matrix elements and computation of ionization spectra we refer to Sections II and III of the Supporting Information.

Fig. 1 shows the experimental⁷¹ and calculated (2-mode) ionization spectra of BT. The two spectra show a nice agreement which validates the 2-mode model.^{69,70} The equilibrium structure of BT (FC point) and body-fixed axis definitions are also visible in Fig. 1. We mention that the interaction between the cavity field and the emitted electron is neglected in the current work. This approximation is justified by the fact that the emitted electron is rather fast (its kinetic energy exceeds 10 eV in the experimental spectrum shown in Fig. 1). On the other hand, investigating the impact of the cavity-electron interaction on the ionization spectrum is of interest by itself, which is left for future work.

Fig. 2 shows different PES cuts. It is clearly visible in panel a of Fig. 2 that the two-dimensional adiabatic (cavity-free) PESs of BT⁺ along normal coordinates Q_t and Q_c form a natural CI at 78447 cm⁻¹ (9.73 eV) above the minimum of the BT ground state. Panel b of Fig. 2 provides one-dimensional BT⁺ PES cuts along Q_t ($Q_c = Q_{\text{TDM}} = Q_{\text{PDM}} = 0$). Besides V_X and V_A one can also see $V_X + \hbar\omega_{\text{cav}}$ and $V_A + \hbar\omega_{\text{cav}}$ in panel b, both shifted by the photon energy with $\omega_{\text{cav}} = 645.02$ cm⁻¹ (~ 0.08 eV). As indicated in panel b, the natural CI at $Q_t = -8.80 \sqrt{m_e}a_0$ (between V_X and V_A) is adjacent to the LICI at $Q_t = -7.04 \sqrt{m_e}a_0$ (between $V_X + \hbar\omega_{\text{cav}}$ and V_A).

Fig. 3 shows computed ionization spectra for $\omega_{\text{cav}} = 645.02$ cm⁻¹ and $g = 0.1$ au (used for visualization purposes only) for the 4-mode model. Results for three different polarizations of the cavity field are depicted in red in Fig. 3. For comparison, ionization spectra of the 4-mode model, but without coupling to the cavity are also shown (blue). The polarization in panel a is $\mathbf{e} = (0, 1, 0)$, i.e., along the y axis. In this case, only the PDMs in the electronic states couple the molecule to the cavity via the ν_{PDM} mode. In panel b the polarization is along the x axis, $\mathbf{e} = (1, 0, 0)$, and the coupling is by the ν_{TDM} mode only. The orthogonality of the TDM to the PDMs enables to control the cavity-induced effects by changing the field polarization and to study the impact of the individual modes on the spectrum. This has been another reason to choose BT for our investigation. The joint impact of the PDM and

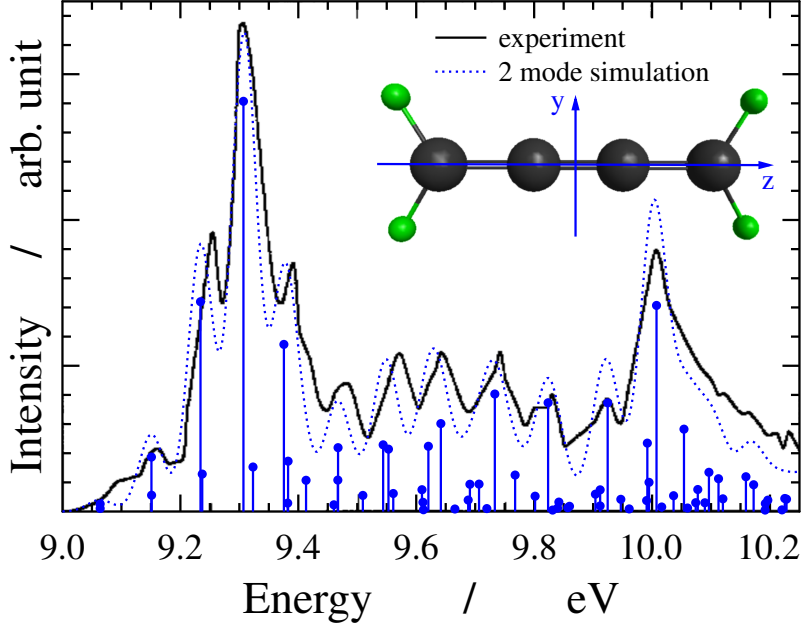


Figure 1. Experimental and calculated (2-mode model) ionization spectra of butatriene (BT), showing nice agreement. See the inset for the equilibrium structure of neutral BT (and body-fixed coordinate axis definitions), corresponding to the Franck–Condon point. The calculated spectral lines are convoluted with a Gaussian function of full width at half maximum of 0.05 eV to account for the experimental resolution.

TDM modes can be studied by varying the polarization in the xy -plane, an example is shown in panel c for $\mathbf{e} = (1, 1, 0)/\sqrt{2}$. In each case, the system is initially assumed to be in the vibrational ground state of BT with zero photons in the cavity which corresponds to the lowest eigenstate of the coupled cavity-molecule system to a very good approximation.

As already stated, the 2-mode vibrational model is insufficient to account for cavity-molecule interactions due to symmetry. However, by making displacements along modes ν_{TDM} and ν_{PDM} the TDM and PDM values are no longer zero and consequently, BT^+ can interact with the cavity mode. More precisely, the coupling to the cavity is induced by dynamical symmetry breaking activated by ionization in the cavity. The impact of the cavity on the ionization process strongly depends on the orientation of the molecule with respect to the field polarization. Accordingly, besides the original ν_c coupling and ν_t tuning modes, ν_{PDM} (only PDM, panel a of Fig. 3), ν_{TDM} (only TDM, panel b), or both ν_{TDM}

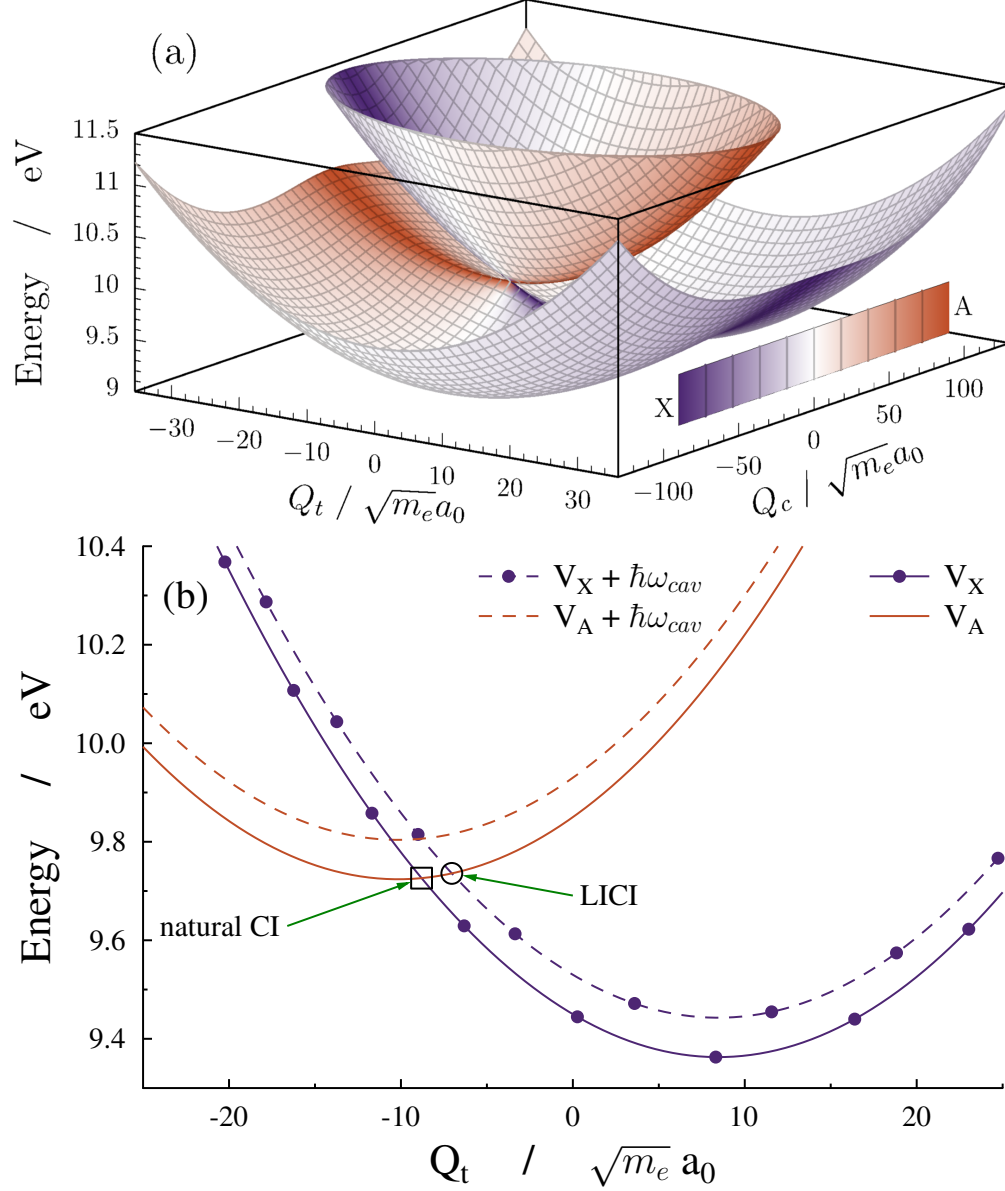


Figure 2. (a) Two-dimensional adiabatic (cavity-free) potential energy surfaces (PESs) of the butatriene cation (BT^+) along the tuning (Q_t) and coupling (Q_c) modes. (b) One-dimensional PES cuts of BT^+ along Q_t with $Q_c = Q_{\text{TDM}} = Q_{\text{PDM}} = 0$. V_X and V_A refer to the ground-state and excited-state PESs of BT^+ , while $V_X + \hbar\omega_{\text{cav}}$ and $V_A + \hbar\omega_{\text{cav}}$ are the same curves shifted by the photon energy with $\omega_{\text{cav}} = 645.02 \text{ cm}^{-1}$ ($\sim 0.08 \text{ eV}$). Positions of the natural conical intersection (CI, between V_X and V_A) and the light-induced conical intersection (LICI, between $V_X + \hbar\omega_{\text{cav}}$ and V_A) are explicitly marked in the figure.

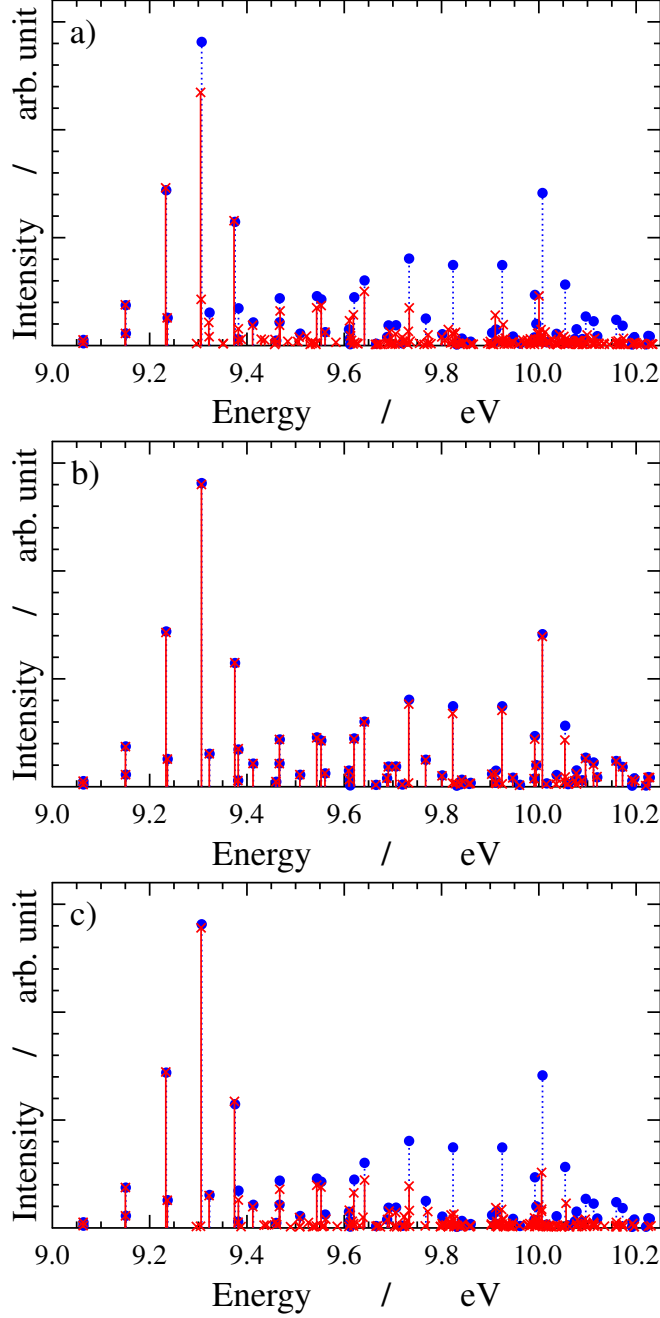


Figure 3. Cavity-free (blue, \bullet) and cavity (red, \times) ionization spectra of butatriene with cavity parameters $\omega_{\text{cav}} = 645.02 \text{ cm}^{-1}$ and $g = 0.1 \text{ au}$. The field polarization vector is chosen in three different ways: $\mathbf{e} = (0, 1, 0)$ (panel a, only permanent dipole moments (PDMs)), $\mathbf{e} = (1, 0, 0)$ (panel b, only transition dipole moment (TDM)), and $\mathbf{e} = (1, 1, 0)/\sqrt{2}$ (panel c, both TDM and PDMs). Significant cavity-induced dynamical effects can be observed mainly in the nonadiabatic region (above 9.55 eV) of the ionization spectrum.

and ν_{PDM} (panel c) come into play. It is conspicuous in Fig. 3 that the cavity-free (blue) and cavity (red) spectra can differ considerably from each other as seen in panels a (only PDM) and c. The impact of ν_{TDM} (panel b) is found to be rather minor in BT^+ . These observations are attributed to the strong mixing by the PDMs of the vibrational levels of the surfaces originating from the solid and dashed blue curves and those originating from the respective red curves in Fig. 2. The resulting hybrid light-matter states are subject to the electronic mixing imposed by the natural CI and are, therefore, expected to strongly change the nonadiabatic effects found in the cavity-free case. Indeed, it is seen in panel a that intense lines in the cavity-free spectrum above about 9.55 eV (blue) are split into many lines of tiny intensities (red).

The energetic position of the natural CI is 9.55 eV above the zero-point energy of BT. Thus, following Ref. 58, the original cavity-free spectrum can be divided into adiabatic ($E < 9.55$ eV) and nonadiabatic ($E > 9.55$ eV) regions. It is apparent in Fig. 3 that the nonadiabatic region is significantly modified by the cavity, while the adiabatic region remains largely unaffected by cavity-molecule interactions (some levels mix in, but their energy splittings are minute). This finding can be rationalized as follows. Nonzero cavity-molecule couplings and cavity effects in the ionization spectrum can be ascribed to dynamical symmetry breaking induced by displacement along modes ν_{TDM} and ν_{PDM} . Owing to the conditions required by the LICI formation (degenerate diabatic potentials and zero cavity-molecule couplings) the LICI is situated near the natural CI for $\omega_{\text{cav}} = 645.02 \text{ cm}^{-1}$ (see panel b of Fig. 2). As a result, the natural CI and the LICI start exerting their effects roughly above the same energy and imprint their signatures in the nonadiabatic region of the cavity-free ionization spectrum, including the mystery band which emerges due to natural nonadiabatic effects. Several additional ionization spectra have been computed, supporting our conclusions. Two of them are shown as examples in Section V of the Supporting Information.

We stress that the natural CI appears again between the surfaces originating from the two dashed curves and the same holds for the LICI which appears again between the red dashed and the blue solid curves (see Fig. 2). This second ‘‘natural CI’’ is actually also a light-induced CI as it does not exist without the cavity. Owing to the low cavity frequency employed, nonadiabatic effects discussed above are due to all of these four conical intersections.

Contrary to BT^+ , many typical molecules possess nonzero TDM and/or PDM values at the FC point. In such cases, there is no need for dynamical symmetry breaking to achieve a strong impact of the cavity on the ionization spectrum. Consequently, the ionization spectrum is expected to show striking cavity-induced effects which one may call static effects, meaning that no dynamical symmetry breaking is involved. In order to demonstrate the emergence of static effects in the ionization spectrum, constant TDM (along the x axis) and PDM (along the y axis) values of 1.0 au are added artificially to the original 2-mode model of BT^+ . Fig. 4 presents cavity ionization spectra for the modified 2-mode model with cavity parameters $\omega_{\text{cav}} = 645.02 \text{ cm}^{-1}$ and $g = 0.002 \text{ au}$ (panel a), and $\omega_{\text{cav}} = 3000.0 \text{ cm}^{-1}$ and $g = 0.01 \text{ au}$ (panel b), both obtained with $\mathbf{e} = (1, 1, 0)/\sqrt{2}$ (both TDM and PDMs are included). As clearly visible in Fig. 4, cavity-induced effects are more pronounced than in Fig. 3 and they affect the entire energy range of the ionization spectra, including the adiabatic region. These observations are remarkable in light of the much lower coupling strengths $g = 0.002 \text{ au}$ and $g = 0.01 \text{ au}$ (used in Fig. 4) compared to $g = 0.1 \text{ au}$ (used in Fig. 3).

We demonstrate the nonadiabatic effects emerging in the cavity by an explicit example. The system of interest is the butatriene cation, BT^+ , which possesses a natural CI between its ground and first excited electronic states near the Franck–Condon (FC) region of the neutral molecule. The natural CI yields a well-separated band (“mystery band”) in the cavity-free ionization spectrum. The 2-mode vibronic coupling model treating a coupling and a tuning vibrational mode has been shown to reproduce the cavity-free low-energy ionization spectrum with good accuracy.⁷⁰ Surprisingly, these two modes do not couple to the cavity and the ionization spectrum within this 2-mode model does not exhibit any impact of the cavity. We show that the cavity activates other modes of the system than these two modes. Including such modes, indeed gives rise to substantial nonadiabatic effects induced by the cavity. The origin of these effects is discussed and analyzed in detail.

In order to generate cavity-molecule interactions, one needs to break the symmetry of BT^+ . This symmetry breaking takes place by the dynamics of the system after ionization and causes noticeable changes primarily in the nonadiabatic region of the ionization spectrum (that is, above the energetic position of the natural CI). This impact of the cavity on the

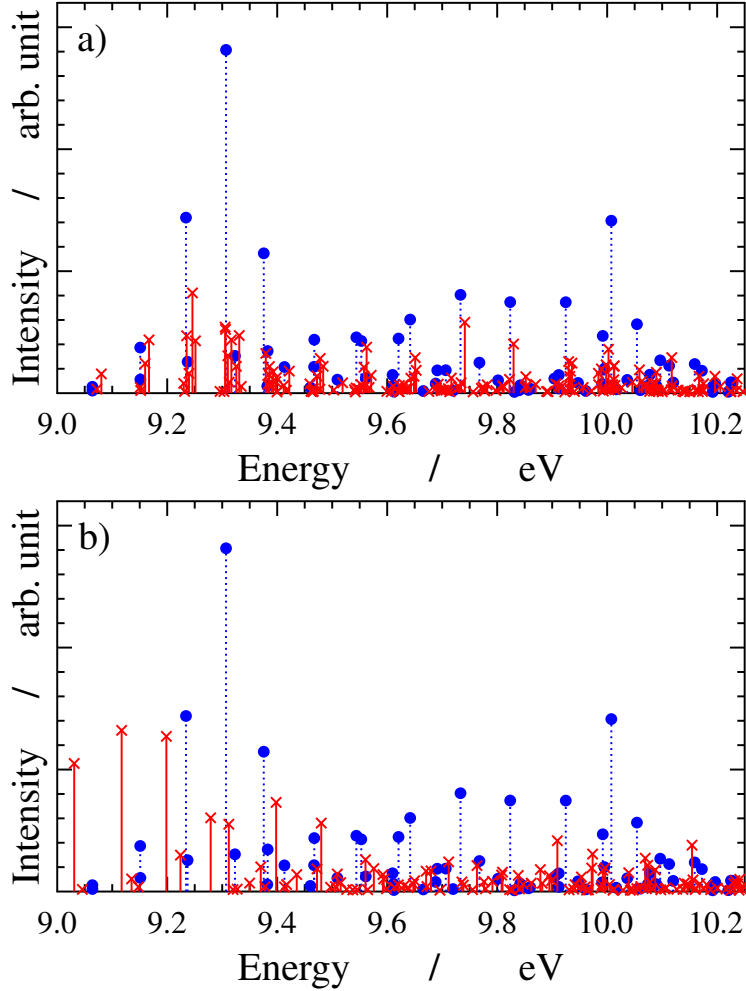


Figure 4. Cavity-free (blue, \bullet) and cavity (red, \times) ionization spectra of butatriene with cavity parameters $\omega_{\text{cav}} = 645.02 \text{ cm}^{-1}$, $g = 0.002 \text{ au}$ (panel a), and $\omega_{\text{cav}} = 3000.0 \text{ cm}^{-1}$, $g = 0.01 \text{ au}$ (panel b). In this case, constant transition (TDM, along the x axis) and permanent (PDM, along the y axis) dipole moment values of 1.0 au are added to the 2-mode model. The field polarization is chosen as $\mathbf{e} = (1, 1, 0)/\sqrt{2}$ (both TDM and PDMs). Significant cavity-induced static effects can be observed in the entire spectral range.

nonadiabatic regime is explained by the proximity of the light-induced CI to the natural CI. Our example, butatriene, has been chosen because of its high symmetry which allows for a transparent discussion of the emerging effects. It should be stressed, however, that strong effects can be expected for molecules of low symmetry. Here, the molecules possess

nonzero transition and/or permanent dipole moments at the FC point and static cavity-induced effects (involving no dynamical symmetry breaking) are already expected to give rise to enormous changes in the entire range of the ionization spectrum. Such effects have been demonstrated in this work.

ACKNOWLEDGMENTS

The authors are indebted to NKFIH for funding (Grant No. K146096). The work performed in Budapest received funding from the HUN-REN Hungarian Research Network. Financial support by the Deutsche Forschungsgemeinschaft (DFG) (Grant No. CE 10/56-1) is gratefully acknowledged.

REFERENCES

- ¹J. A. Hutchison, T. Schwartz, C. Genet, E. Devaux, and T. W. Ebbesen, “Modifying chemical landscapes by coupling to vacuum fields,” *Angew. Chem. Int. Ed.* **51**, 1592–1596 (2012).
- ²T. Ebbesen, “Hybrid light-matter states in a molecular and material science perspective,” *Acc. Chem. Res.* **49**, 2403–2412 (2016).
- ³R. Chikkaraddy, B. De Nijs, F. Benz, S. Barrow, O. Scherman, E. Rosta, A. Demetriadou, P. Fox, O. Hess, and J. Baumberg, “Single-molecule strong coupling at room temperature in plasmonic nanocavities,” *Nature* **535**, 127–130 (2016).
- ⁴M. Kowalewski, K. Bennett, and S. Mukamel, “Cavity femtochemistry: Manipulating nonadiabatic dynamics at avoided crossings,” *J. Phys. Chem. Lett.* **7**, 2050–2054 (2016).
- ⁵J. Flick, M. Ruggenthaler, H. Appel, and A. Rubio, “Atoms and molecules in cavities, from weak to strong coupling in quantum-electrodynamics (QED) chemistry,” *Proc. Natl. Acad. Sci. U.S.A.* **114**, 3026–3034 (2017).
- ⁶J. Feist, J. Galego, and F. Garcia-Vidal, “Polaritonic chemistry with organic molecules,” *ACS Photonics* **5**, 205–216 (2018).

- ⁷J. Fregoni, G. Granucci, E. Coccia, M. Persico, and S. Corni, “Manipulating azobenzene photoisomerization through strong light-molecule coupling,” *Nat. Commun.* **9**, 4688 (2018).
- ⁸R. Ribeiro, L. Martínez-Martínez, M. Du, J. Campos-Gonzalez-Angulo, and J. Yuen-Zhou, “Polariton chemistry: Controlling molecular dynamics with optical cavities,” *Chem. Sci.* **9**, 6325–6339 (2018).
- ⁹T. Szidarovszky, G. Halász, A. Császár, L. Cederbaum, and Á. Vibók, “Conical intersections induced by quantum light: Field-dressed spectra from the weak to the ultrastrong coupling regimes,” *J. Phys. Chem. Lett.* **9**, 6215–6223 (2018).
- ¹⁰M. Ruggenthaler, N. Tancogne-Dejean, J. Flick, H. Appel, and A. Rubio, “From a quantum-electrodynamical light-matter description to novel spectroscopies,” *Nat. Rev. Chem.* **2**, 0118 (2018).
- ¹¹O. Vendrell, “Collective Jahn-Teller interactions through light-matter coupling in a cavity,” *Phys. Rev. Lett.* **121**, 253001 (2018).
- ¹²A. Csehi, Á. Vibók, G. Halász, and M. Kowalewski, “Quantum control with quantum light of molecular nonadiabaticity,” *Phys. Rev. A* **100**, 053421 (2019).
- ¹³A. Csehi, M. Kowalewski, G. Halász, and Á. Vibók, “Ultrafast dynamics in the vicinity of quantum light-induced conical intersections,” *New J. Phys.* **21**, 093040 (2019).
- ¹⁴M. Reitz, C. Sommer, and C. Genes, “Langevin approach to quantum optics with molecules,” *Phys. Rev. Lett.* **122**, 203602 (2019).
- ¹⁵I. Ulusoy, J. Gomez, and O. Vendrell, “Modifying the nonradiative decay dynamics through conical intersections via collective coupling to a cavity mode,” *J. Phys. Chem. A* **123**, 8832–8844 (2019).
- ¹⁶A. Mandal and P. Huo, “Investigating new reactivities enabled by polariton photochemistry,” *J. Phys. Chem. Lett.* **10**, 5519–5529 (2019).
- ¹⁷J. Triana and J. Sanz-Vicario, “Revealing the presence of potential crossings in diatomics induced by quantum cavity radiation,” *Phys. Rev. Lett.* **122**, 063603 (2019).
- ¹⁸J. Yuen-Zhou and V. M. Menon, “Polariton chemistry: Thinking inside the (photon) box,” *Proc. Natl. Acad. Sci. U.S.A.* **116**, 5214–5216 (2019).
- ¹⁹E. Davidsson and M. Kowalewski, “Simulating photodissociation reactions in bad cavities with the Lindblad equation,” *J. Chem. Phys.* **153**, 234304 (2020).

- ²⁰C. Fábri, B. Lasorne, G. Halász, L. Cederbaum, and Á. Vibók, “Quantum light-induced nonadiabatic phenomena in the absorption spectrum of formaldehyde: Full- and reduced-dimensionality studies,” *J. Chem. Phys.* **153**, 234302 (2020).
- ²¹B. Gu and S. Mukamel, “Manipulating nonadiabatic conical intersection dynamics by optical cavities,” *Chem. Sci.* **11**, 1290–1298 (2020).
- ²²B. Gu and S. Mukamel, “Cooperative conical intersection dynamics of two pyrazine molecules in an optical cavity,” *J. Phys. Chem. Lett.* **11**, 5555–5562 (2020).
- ²³R. Silva, J. Pino, F. García-Vidal, and J. Feist, “Polaritonic molecular clock for all-optical ultrafast imaging of wavepacket dynamics without probe pulses,” *Nat. Commun.* **11**, 1423 (2020).
- ²⁴S. Felicetti, J. Fregoni, T. Schnappinger, S. Reiter, R. De Vivie-Riedle, and J. Feist, “Photoprotecting uracil by coupling with lossy nanocavities,” *J. Phys. Chem. Lett.* **11**, 8810–8818 (2020).
- ²⁵J. Fregoni, G. Granucci, M. Persico, and S. Corni, “Strong coupling with light enhances the photoisomerization quantum yield of azobenzene,” *Chem* **6**, 250–265 (2020).
- ²⁶A. Mandal, T. D. Krauss, and P. Huo, “Polariton-mediated electron transfer via cavity quantum electrodynamics,” *J. Phys. Chem. B* **124**, 6321–6340 (2020).
- ²⁷D. Polak, R. Jayaprakash, T. P. Lyons, L. Á. Martínez-Martínez, A. Leventis, K. J. Fallon, H. Coulthard, D. G. Bossanyi, K. Georgiou, A. J. Petty, II, J. Anthony, H. Bronstein, J. Yuen-Zhou, A. I. Tartakovskii, J. Clark, and A. J. Musser, “Manipulating molecules with strong coupling: Harvesting triplet excitons in organic exciton microcavities,” *Chem. Sci.* **11**, 343–354 (2020).
- ²⁸C. Fábri, G. Halász, L. Cederbaum, and Á. Vibók, “Born-Oppenheimer approximation in optical cavities: From success to breakdown,” *Chem. Sci.* **12**, 1251–1258 (2021).
- ²⁹F. J. Garcia-Vidal, C. Ciuti, and T. W. Ebbesen, “Manipulating matter by strong coupling to vacuum fields,” *Science* **373**, eabd0336 (2021).
- ³⁰C. Huang, A. Ahrens, M. Beutel, and K. Varga, “Two electrons in harmonic confinement coupled to light in a cavity,” *Phys. Rev. B* **104**, 165147 (2021).
- ³¹T. Szidarovszky, P. Badankó, G. J. Halász, and Á. Vibók, “Nonadiabatic Phenomena in Molecular Vibrational Polaritons,” *J. Chem. Phys.* **154**, 064305 (2021).

- ³²L. S. Cederbaum and A. I. Kuleff, “Impact of cavity on interatomic coulombic decay,” *Nat. Commun.* **12**, 4083 (2021).
- ³³L. S. Cederbaum, “Polaritonic states of matter in a rotating cavity,” *J. Phys. Chem. Lett.* **12**, 6056–6061 (2021).
- ³⁴C. Schäfer, F. Buchholz, M. Penz, M. Ruggenthaler, and A. Rubio, “Making ab initio QED functional(s): Nonperturbative and photon-free effective frameworks for strong light-matter coupling,” *Proc. Natl. Acad. Sci. U.S.A.* **118**, e2110464118 (2021).
- ³⁵J. Triana and J. Sanz-Vicario, “Polar diatomic molecules in optical cavities: Photon scaling, rotational effects, and comparison with classical fields,” *J. Chem. Phys.* **154**, 094120 (2021).
- ³⁶E. W. Fischer and P. Saalfrank, “Ground state properties and infrared spectra of anharmonic vibrational polaritons of small molecules in cavities,” *J. Chem. Phys.* **154**, 104311 (2021).
- ³⁷M. H. Farag, A. Mandal, and P. Huo, “Polariton induced conical intersection and berry phase,” *Phys. Chem. Chem. Phys.* **23**, 16868–16879 (2021).
- ³⁸C. Fábri, G. J. Halász, and Á. Vibók, “Probing light-induced conical intersections by monitoring multidimensional polaritonic surfaces,” *J. Phys. Chem. Lett.* **13**, 1172–1179 (2022).
- ³⁹C. Schäfer, “Polaritonic chemistry from first principles via embedding radiation reaction,” *J. Phys. Chem. Lett.* **13**, 6905–6911 (2022).
- ⁴⁰E. W. Fischer and P. Saalfrank, “Cavity-induced non-adiabatic dynamics and spectroscopy of molecular rovibrational polaritons studied by multi-mode quantum models,” *J. Chem. Phys.* **157**, 034305 (2022).
- ⁴¹T. E. Li, B. Cui, J. E. Subotnik, and A. Nitzan, “Molecular polaritonics: Chemical dynamics under strong light–matter coupling,” *Annu. Rev. Phys. Chem.* **73**, 43–71 (2022).
- ⁴²B. Cui and A. Nitzan, “Collective response in light-matter interactions: The interplay between strong coupling and local dynamics,” *J. Chem. Phys.* **157**, 114108 (2022).
- ⁴³D. Wellnitz, G. Pupillo, and J. Schachenmayer, “Disorder enhanced vibrational entanglement and dynamics in polaritonic chemistry,” *Commun. Phys.* **5**, 120 (2022).
- ⁴⁴J. Malave, Y. S. Akililu, M. Beutel, C. Huang, and K. Varga, “Harmonically confined N -electron systems coupled to light in a cavity,” *Phys. Rev. B* **105**, 115127 (2022).

- ⁴⁵M. Reitz, C. Sommer, and C. Genes, “Cooperative quantum phenomena in light-matter platforms,” *PRX Quantum* **3**, 010201 (2022).
- ⁴⁶J. Fregoni, F. J. Garcia-Vidal, and J. Feist, “Theoretical challenges in polaritonic chemistry,” *ACS Photonics* **9**, 1096–1107 (2022).
- ⁴⁷O. Bitton and G. Haran, “Plasmonic cavities and individual quantum emitters in the strong coupling limit,” *Acc. Chem. Res.* **55**, 1659–1668 (2022).
- ⁴⁸L.-B. Fan, C.-C. Shu, D. Dong, J. He, N. E. Henriksen, and F. Nori, “Quantum coherent control of a single molecular-polariton rotation,” *Phys. Rev. Lett.* **130**, 043604 (2023).
- ⁴⁹T. Schnappinger and M. Kowalewski, “Nonadiabatic wave packet dynamics with ab initio cavity-born-oppenheimer potential energy surfaces,” *J. Chem. Theory Comput.* **19**, 460–471 (2023).
- ⁵⁰A. Koner, M. Du, S. Pannir-Sivajothi, R. H. Goldsmith, and J. Yuen-Zhou, “A path towards single molecule vibrational strong coupling in a Fabry-Pérot microcavity,” *Chem. Sci.* **14**, 7753–7761 (2023).
- ⁵¹C. Schäfer, M. Ruggenthaler, V. Rokaj, and A. Rubio, “Relevance of the quadratic diamagnetic and self-polarization terms in cavity quantum electrodynamics,” *ACS Photonics* **7**, 975–990 (2020).
- ⁵²A. Mandal, S. Montillo Vega, and P. Huo, “Polarized Fock states and the dynamical Casimir effect in molecular cavity quantum electrodynamics,” *J. Phys. Chem. Lett.* **11**, 9215–9223 (2020).
- ⁵³M. A. D. Taylor, A. Mandal, W. Zhou, and P. Huo, “Resolution of gauge ambiguities in molecular cavity quantum electrodynamics,” *Phys. Rev. Lett.* **125**, 123602 (2020).
- ⁵⁴J. Galego, F. J. Garcia-Vidal, and J. Feist, “Suppressing photochemical reactions with quantized light fields,” *Nat. Commun.* **7**, 13841 (2016).
- ⁵⁵T. Szidarovszky, G. J. Halász, and Á. Vibók, “Three-player polaritons: Nonadiabatic fingerprints in an entangled atom-molecule-photon system,” *New J. Phys.* **22**, 053001 (2020).
- ⁵⁶C. Fábri, G. J. Halász, L. S. Cederbaum, and Á. Vibók, “Radiative emission of polaritons controlled by light-induced geometric phase,” *Chem. Commun.* **58**, 12612–12615 (2022).
- ⁵⁷A. Csehi, O. Vendrell, G. J. Halász, and Á. Vibók, “Competition between collective and individual conical intersection dynamics in an optical cavity,” *New J. Phys.* **24**, 073022

- (2022).
- ⁵⁸H. Köppel, W. Domcke, and L. S. Cederbaum, “Multimode molecular dynamics beyond the Born–Oppenheimer approximation,” *Adv. Chem. Phys.* **57**, 59–246 (1984).
- ⁵⁹D. Yarkony, “Diabolical conical intersections,” *Rev. Mod. Phys.* **68**, 985–1013 (1996).
- ⁶⁰M. Baer, “Introduction to the theory of electronic non-adiabatic coupling terms in molecular systems,” *Phys. Rep.* **358**, 75–142 (2002).
- ⁶¹W. Domcke, D. R. Yarkony, and H. Köppel, *Conical Intersections: Electronic Structure, Dynamics and Spectroscopy* (World Scientific, Singapore, 2004).
- ⁶²G. Worth and L. Cederbaum, “Beyond born-oppenheimer: Molecular dynamics through a conical intersection,” *Annu. Rev. Phys. Chem.* **55**, 127–158 (2004).
- ⁶³M. Baer, *Beyond Born-Oppenheimer: Electronic Nonadiabatic Coupling Terms and Conical Intersections* (John Wiley & Sons: Hoboken, NJ, 2006).
- ⁶⁴M. Šindelka, N. Moiseyev, and L. S. Cederbaum, “Strong impact of light-induced conical intersections on the spectrum of diatomic molecules,” *J. Phys. B: At. Mol. Opt. Phys.* **44**, 045603 (2011).
- ⁶⁵G. Halász, Á. Vibók, and L. Cederbaum, “Direct signature of light-induced conical intersections in diatomics,” *J. Phys. Chem. Lett.* **6**, 348–354 (2015).
- ⁶⁶P. Badankó, O. Umarov, C. Fábri, G. Halász, and Á. Vibók, “Topological aspects of cavity-induced degeneracies in polyatomic molecules,” *Int. J. Quantum Chem.* **122**, e26750 (2022).
- ⁶⁷A. E. DePrince III, “Cavity-modulated ionization potentials and electron affinities from quantum electrodynamics coupled-cluster theory,” *J. Chem. Phys.* **154**, 094112 (2021).
- ⁶⁸R. R. Riso, T. S. Haugland, E. Ronca, and H. Koch, “On the characteristic features of ionization in QED environments,” *J. Chem. Phys.* **156**, 234103 (2022).
- ⁶⁹L. Cederbaum, W. Domcke, H. Köppel, and W. Von Niessen, “Strong vibronic coupling effects in ionization spectra: The “mystery band” of butatriene,” *Chem. Phys.* **26**, 169–177 (1977).
- ⁷⁰C. Cattarius, G. A. Worth, H.-D. Meyer, and L. S. Cederbaum, “All mode dynamics at the conical intersection of an octa-atomic molecule: Multi-configuration time-dependent Hartree (MCTDH) investigation on the butatriene cation,” *J. Chem. Phys.* **115**, 2088–2100 (2001).

- ⁷¹F. Brogli, E. Heilbronner, E. Kloster-Jensen, A. Schmelzer, A. Manocha, J. Pople, and L. Radom, “The photoelectron spectrum of butatriene,” *Chem. Phys.* **4**, 107–119 (1974).
- ⁷²C. Cohen-Tannoudji, J. Dupont-Roc, and G. Grynberg, *Atom-Photon Interactions: Basic Processes and Applications* (Wiley-VCH Verlag GmbH and Co. KGaA, Weinheim, 2004).
- ⁷³J. Galego, C. Climent, F. J. Garcia-Vidal, and J. Feist, “Cavity Casimir-Polder forces and their effects in ground-state chemical reactivity,” *Phys. Rev. X* **9**, 021057 (2019).
- ⁷⁴J. Feist, A. I. Fernández-Domínguez, and F. J. García-Vidal, “Macroscopic QED for quantum nanophotonics: Emitter-centered modes as a minimal basis for multiemitter problems,” *Nanophotonics* **10**, 477–489 (2021).
- ⁷⁵V. Rokaj, D. M. Welakuh, M. Ruggenthaler, and A. Rubio, “Light-matter interaction in the long-wavelength limit: No ground-state without dipole self-energy,” *J. Phys. B: At. Mol. Opt. Phys.* **51**, 034005 (2018).
- ⁷⁶M. L. Weichman, L. Cheng, J. B. Kim, J. F. Stanton, and D. M. Neumark, “Low-lying vibronic level structure of the ground state of the methoxy radical: Slow electron velocity-map imaging (SEVI) spectra and Köppel-Domcke-Cederbaum (KDC) vibronic Hamiltonian calculations,” *J. Chem. Phys.* **146**, 224309 (2017).

Supporting Information

I. DESCRIPTION OF THE MOLECULE AND GROUP-THEORETICAL CONSIDERATIONS

The planar equilibrium structure of butatriene (Franck–Condon (FC) point), shown in Fig. 5, is of D_{2h} symmetry. The character table of the D_{2h} point group is provided in Table I. The two lowest electronic states X and A of the cation have $\Gamma_X = B_{2g}$ and $\Gamma_A = B_{2u}$ symmetries at the FC point, respectively. Following Ref. 70 of the manuscript, the 18 vibrational modes of butatriene can be classified by D_{2h} irreducible representations (irreps) as

$$\Gamma_{\text{vib}} = 4A_g \oplus A_u \oplus 2B_{2g} \oplus 3B_{3g} \oplus 3B_{1u} \oplus 3B_{2u} \oplus 2B_{3u}. \quad (4)$$

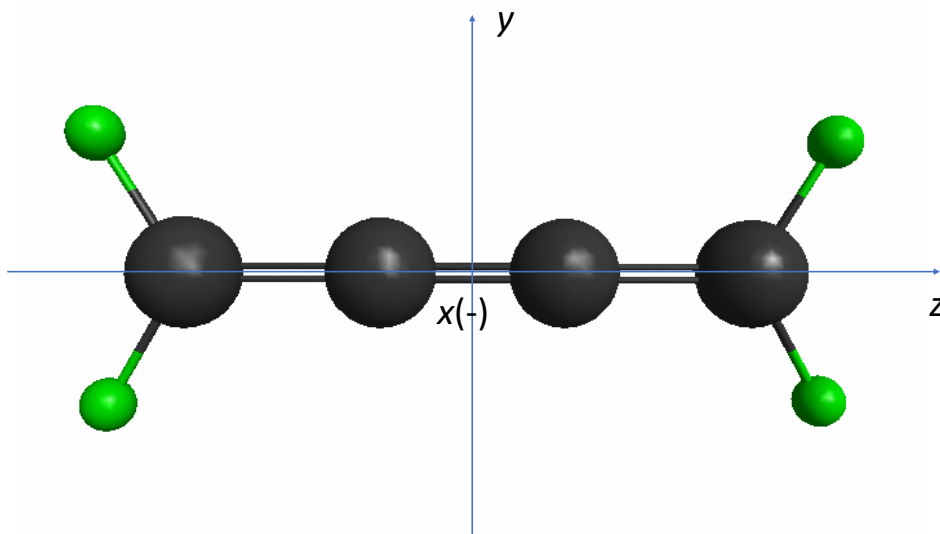


Figure 5. Equilibrium structure of the neutral butatriene (C_4H_4) molecule and definition of the body-fixed Cartesian axes. The minus sign indicates that the x axis is directed inward.

Using the body-fixed axis definitions in Fig. 5, we get that the x , y and z coordinates transform according to the irreps

$$\Gamma_x = B_{3u} \quad \Gamma_y = B_{2u} \quad \Gamma_z = B_{1u}. \quad (5)$$

Table I. Character table of the D_{2h} point group.

	E	$C_2(z)$	$C_2(y)$	$C_2(x)$	i	$\sigma(xy)$	$\sigma(xz)$	$\sigma(yz)$
A_g	1	1	1	1	1	1	1	1
B_{1g}	1	1	-1	-1	1	1	-1	-1
B_{2g}	1	-1	1	-1	1	-1	1	-1
B_{3g}	1	-1	-1	1	1	-1	-1	1
A_u	1	1	1	1	-1	-1	-1	-1
B_{1u}	1	1	-1	-1	-1	-1	1	1
B_{2u}	1	-1	1	-1	-1	1	-1	1
B_{3u}	1	-1	-1	1	-1	1	1	-1

Since the direct product representations

$$\begin{aligned}
 \Gamma_X \otimes \Gamma_x \otimes \Gamma_A &= B_{2g} \otimes B_{3u} \otimes B_{2u} = B_{3g} \\
 \Gamma_X \otimes \Gamma_y \otimes \Gamma_A &= B_{2g} \otimes B_{2u} \otimes B_{2u} = B_{2g} \\
 \Gamma_X \otimes \Gamma_z \otimes \Gamma_A &= B_{2g} \otimes B_{1u} \otimes B_{2u} = B_{1g}
 \end{aligned} \tag{6}$$

do not contain the totally symmetric irrep A_g , all components of the transition dipole moment (TDM) between the X $^2B_{2g}$ and A $^2B_{2u}$ states vanish at the FC point. Using similar arguments one can easily show that the X $^2B_{2g}$ and A $^2B_{2u}$ permanent dipole moments (PDMs) are also zero at the FC point, for example, one gets

$$\begin{aligned}
 \Gamma_X \otimes \Gamma_x \otimes \Gamma_X &= B_{2g} \otimes B_{3u} \otimes B_{2g} = B_{3u} \\
 \Gamma_X \otimes \Gamma_y \otimes \Gamma_X &= B_{2g} \otimes B_{2u} \otimes B_{2g} = B_{2u} \\
 \Gamma_X \otimes \Gamma_z \otimes \Gamma_X &= B_{2g} \otimes B_{1u} \otimes B_{2g} = B_{1u}
 \end{aligned} \tag{7}$$

for the X $^2B_{2g}$ state.

It is evident from Eq. (6) that displacement along a given B_{3g} or B_{2g} vibrational mode has to be made to produce nonzero TDM along the body-fixed x and y axes, respectively. Since according to Eq. (4) there is no B_{1g} mode, simultaneous displacements along a B_{3g} and a B_{2g} mode are required to produce TDM along the body-fixed z axis. Similar rules can

Table II. Experimental (ω_{exp}) and calculated (ω_{calc} , MP2/D95** level of theory) harmonic wavenumbers in units of cm^{-1} , symmetry labels (D_{2h} point group) and qualitative descriptions of the vibrational modes relevant for the current study. Harmonic wavenumbers used in numerical computations are set in bold.

mode	symmetry	$\omega_{\text{exp}} / \text{cm}^{-1}$	$\omega_{\text{calc}} / \text{cm}^{-1}$	description
ν_{14}	A_g	2079.30	2157.27	C–C stretch (central)
ν_5	A_u	735.58	777.57	torsion
ν_9	B_{3g}	662.99	1014.34	CH ₂ rocking
ν_{10}	B_{2u}	1059.81	1050.12	CH ₂ rocking

be derived for PDM components along the same lines, namely, displacements along B_{3u} , B_{2u} and B_{1u} modes generate PDMs along the body-fixed x , y and z axes, respectively.

Finally, vibrational modes relevant for the current study are described in Table II. As discussed in the next section, the modes ν_{14} and ν_5 play the role of the tuning (ν_t) and coupling (ν_c) modes, respectively. In addition to ν_t and ν_c , we choose modes ν_9 (ν_{TDM}) and ν_{10} (ν_{PDM}) to generate TDM and PDMs along the x and y axes. This way, ν_{TDM} and ν_{PDM} give rise to cavity-molecule couplings upon displacement from the FC point.

II. DESCRIPTION OF THE 2-MODE VIBRONIC COUPLING MODEL

In this section the 2-mode vibronic coupling model is briefly summarized where vibrational modes ν_5 and ν_{14} correspond to the coupling (ν_c) and tuning (ν_t) modes, respectively. The ground electronic state of the neutral molecule is described by the harmonic oscillator Hamiltonian

$$\hat{H}_0^{\text{neutral,2D}} = \hat{T} + V \quad (8)$$

with

$$\hat{T} = -\frac{1}{2} \sum_{i=c,t} \frac{\partial^2}{\partial Q_i^2} \quad (9)$$

and

$$V = \frac{1}{2} \sum_{i=c,t} \omega_i^2 Q_i^2 \quad (10)$$

where Q_c and Q_t refer to normal coordinates associated with the coupling and tuning modes, respectively and \hbar is set to one. The ground (X) and first excited (A) electronic states are taken into account for the cation, which yields the diabatic Hamiltonian

$$\hat{H}_0^{\text{ion},2\text{D}} = \begin{bmatrix} \hat{T} & 0 \\ 0 & \hat{T} \end{bmatrix} + \begin{bmatrix} V_X & V_{XA} \\ V_{XA} & V_A \end{bmatrix} \quad (11)$$

with

$$V_X = \epsilon_X + \frac{1}{2} \sum_{i=c,t} \omega_i^2 Q_i^2 + \kappa_X Q_t, \quad (12)$$

$$V_A = \epsilon_A + \frac{1}{2} \sum_{i=c,t} \omega_i^2 Q_i^2 + \kappa_A Q_t \quad (13)$$

and

$$V_{XA} = \lambda Q_c. \quad (14)$$

The model parameters ($\epsilon_{X/A}$, ω_i , $\kappa_{X/A}$, λ) have been taken from Ref. 70 of the manuscript.

Next, a numerical method is presented for solving the eigenproblem of $\hat{H}_0^{\text{ion},2\text{D}}$. The eigenstates of $\hat{H}_0^{\text{ion},2\text{D}}$ are expressed as two-component vectors, that is,

$$|\vec{\psi}(Q_c, Q_t)\rangle = \begin{bmatrix} |\psi_X(Q_c, Q_t)\rangle \\ |\psi_A(Q_c, Q_t)\rangle \end{bmatrix} \quad (15)$$

which is equivalent to the expansion $|\psi(Q_c, Q_t)\rangle = |\psi_X(Q_c, Q_t)\rangle|X\rangle + |\psi_A(Q_c, Q_t)\rangle|A\rangle$. Components of $|\vec{\psi}(Q_c, Q_t)\rangle$ can be expanded in a product basis of 1D harmonic-oscillator eigenfunctions of the neutral ground state,

$$|\psi_\alpha(Q_c, Q_t)\rangle = \sum_{v_c, v_t} c_{v_c, v_t}^\alpha |\varphi_{v_c}(Q_c)\rangle |\varphi_{v_t}(Q_t)\rangle \quad (16)$$

with $\alpha = X, A$. Matrix elements of $\hat{H}_0^{\text{ion},2\text{D}}$ in the basis defined in Eq. (16) read

$$\begin{aligned} \langle \varphi_{v'_c} \varphi_{v'_t} | \hat{T} + V_\alpha | \varphi_{v_c} \varphi_{v_t} \rangle &= \left[\epsilon_\alpha + \omega_c \left(v_c + \frac{1}{2} \right) + \omega_t \left(v_t + \frac{1}{2} \right) \right] \delta_{v'_c, v_c} \delta_{v'_t, v_t} \\ &+ \kappa_\alpha \langle \varphi_{v'_t} | Q_t | \varphi_{v_t} \rangle \delta_{v'_c, v_c} \end{aligned} \quad (17)$$

for the diagonal blocks ($\alpha = X, A$) and

$$\langle \varphi_{v'_c} \varphi_{v'_t} | V_{XA} | \varphi_{v_c} \varphi_{v_t} \rangle = \lambda \langle \varphi_{v'_c} | Q_c | \varphi_{v_c} \rangle \delta_{v'_t, v_t} \quad (18)$$

for the offdiagonal block of $\hat{H}_0^{\text{ion}, 2D}$. In Eq. (18), coordinate matrix elements for the coupling mode can be obtained as

$$\langle \varphi_{v'_c} | Q_c | \varphi_{v_c} \rangle = \frac{1}{\sqrt{2\omega_c}} (\sqrt{v_c + 1} \delta_{v'_c, v_c+1} + \sqrt{v_c} \delta_{v'_c, v_c-1}). \quad (19)$$

Coordinate matrix elements for the tuning mode in Eq. (17) can be expressed in the same fashion.

Finally, a brief description of the computation of the ionization spectrum is provided. The initial state is assumed to be the vibrational ground state of the neutral molecule in its electronic ground state,

$$|\psi_i(Q_c, Q_t)\rangle = |\varphi_0(Q_c)\rangle |\varphi_0(Q_t)\rangle \quad (20)$$

where the harmonic-oscillator approximation is applied, see Eq. (8). The final states correspond to eigenstates $|\vec{\psi}_f(Q_c, Q_t)\rangle$ of the cation defined in Eq. (15). Assuming that ionization probabilities of the neutral ground state are nuclear-position independent and equal for the cationic states X and A we get

$$A_{\text{if}} = \sum_{\alpha=X,A} \langle \psi_i(Q_c, Q_t) | \psi_{f,\alpha}(Q_c, Q_t) \rangle \quad (21)$$

for the transition amplitudes. Transition probabilities I_{if} are proportional to transition wavenumbers ω_{if} and absolute squares of transition amplitudes A_{if} , that is, $I_{\text{if}} \propto \omega_{\text{if}} |A_{\text{if}}|^2$.

III. DESCRIPTION OF THE 4-MODE MODEL FOR THE COUPLED CAVITY-MOLECULE SYSTEM

The Hamiltonian of the cation coupled to a single cavity mode has the form

$$\hat{H}_{\text{cm}} = \hat{H}_0^{\text{ion}} + \hbar\omega_{\text{cav}} \hat{a}^\dagger \hat{a} - g\hat{\mu}\vec{e}(\hat{a}^\dagger + \hat{a}) \quad (22)$$

which, taking into account the two lowest electronic states (X and A), can be recast as

$$\hat{H}_{\text{cm}} = \begin{bmatrix} \hat{T} + V_X & V_{XA} & -g\mu_X & -g\mu_{XA} & 0 & 0 & \dots \\ V_{XA} & \hat{T} + V_A & -g\mu_{XA} & -g\mu_A & 0 & 0 & \dots \\ -g\mu_X & -g\mu_{XA} & \hat{T} + V_X + \hbar\omega_{\text{cav}} & V_{XA} & -g\sqrt{2}\mu_X & -g\sqrt{2}\mu_{XA} & \dots \\ -g\mu_{XA} & -g\mu_A & V_{XA} & \hat{T} + V_A + \hbar\omega_{\text{cav}} & -g\sqrt{2}\mu_{XA} & -g\sqrt{2}\mu_A & \dots \\ 0 & 0 & -g\sqrt{2}\mu_X & -g\sqrt{2}\mu_{XA} & \hat{T} + V_X + 2\hbar\omega_{\text{cav}} & V_{XA} & \dots \\ 0 & 0 & -g\sqrt{2}\mu_{XA} & -g\sqrt{2}\mu_A & V_{XA} & \hat{T} + V_A + 2\hbar\omega_{\text{cav}} & \dots \\ \vdots & \vdots & \vdots & \vdots & \vdots & \vdots & \ddots \end{bmatrix} \quad (23)$$

where ω_{cav} , g , $\hat{\vec{\mu}}$ and \vec{e} are the cavity angular frequency, coupling strength parameter, electric dipole moment of the molecule and polarization vector of the cavity field, respectively, while \hat{a}^\dagger and \hat{a} denote creation and annihilation operators of the cavity mode. In addition, PDM and TDM components along \vec{e} are denoted by μ_α ($\alpha = X, A$) and μ_{XA} , respectively.

In order to produce nonzero TDM and PDMs, $\hat{H}_0^{\text{ion},2\text{D}}$ of Eq. (11) is supplemented with two additional vibrational modes, which yields

$$\hat{H}_0^{\text{ion}} = \begin{bmatrix} \hat{T} & 0 \\ 0 & \hat{T} \end{bmatrix} + \begin{bmatrix} V_X & V_{XA} \\ V_{XA} & V_A \end{bmatrix} \quad (24)$$

with

$$\hat{T} = -\frac{1}{2} \sum_{\substack{i=\text{c,t}, \\ \text{TDM,PDM}}} \frac{\partial^2}{\partial Q_i^2}, \quad (25)$$

$$V_X = \epsilon_X + \frac{1}{2} \sum_{\substack{i=\text{c,t}, \\ \text{TDM,PDM}}} \omega_i^2 Q_i^2 + \kappa_X Q_t, \quad (26)$$

$$V_A = \epsilon_A + \frac{1}{2} \sum_{\substack{i=\text{c,t}, \\ \text{TDM,PDM}}} \omega_i^2 Q_i^2 + \kappa_A Q_t \quad (27)$$

and

$$V_{XA} = \lambda Q_c. \quad (28)$$

The group-theoretical analysis presented in Section I suggests that the PDM and TDM

functions can be approximated by the expansions

$$\begin{aligned}\mu_X &= \beta_X Q_{\text{PDM}} \\ \mu_A &= \beta_A Q_{\text{PDM}} \\ \mu_{\text{XA}} &= \gamma Q_{\text{TDM}}\end{aligned}\tag{29}$$

where β_X , β_A and γ are constants.

Eigenstates of the coupled cavity-molecule system are constructed as

$$|\vec{\Phi}_k\rangle = \begin{bmatrix} \sum_{\mathbf{v}} \sum_n b_{\mathbf{v},n}^{X,k} |\mathbf{v}\rangle |n\rangle \\ \sum_{\mathbf{v}} \sum_n b_{\mathbf{v},n}^{A,k} |\mathbf{v}\rangle |n\rangle \end{bmatrix}\tag{30}$$

where $|n\rangle$ refers to Fock states of the cavity mode and $|\mathbf{v}\rangle = |v_c, v_t, v_{\text{TDM}}, v_{\text{PDM}}\rangle$ denotes four-dimensional harmonic-oscillator basis states. The matrix representation of \hat{H}_{cm} (see Eq. (23)) is set up using the basis defined in Eq. (30) and the resulting Hamiltonian matrix is diagonalized with a sparse eigensolver. Regarding the ionization spectrum, the initial state is assumed to be the vibrational ground state of the neutral molecule in its electronic ground state with zero photons in the cavity, that is,

$$|\Phi_0\rangle = |\mathbf{0}\rangle |0\rangle.\tag{31}$$

With these quantities at hand transition amplitudes from $|\Phi_0\rangle$ to $|\vec{\Phi}_k\rangle$ (see Eq. (30)) are expressed as

$$A_{0k} = \sum_{\alpha=X,A} \langle \Phi_0 | \Phi_{k,\alpha} \rangle.\tag{32}$$

IV. TECHNICAL DETAILS OF THE COMPUTATIONS

A. Ab initio calculations and model parameters

Following Ref. 70 of the manuscript, the equilibrium geometry of neutral butatriene was optimized at the MP2/D95** level of theory with the Gaussian 16 program. Normal coordinates were constructed by diagonalizing the mass-weighted Cartesian Hessian and used in subsequent nuclear motion computations. Vibrational modes relevant for the current study

are summarized in Table II where harmonic wavenumbers used in numerical computations are set in bold. Other model parameters, taken from Ref. 70 of the manuscript, are as follows: $\epsilon_X = 9.45$ eV, $\epsilon_A = 9.85$ eV, $\kappa_X = -0.212$ eV, $\kappa_A = 0.255$ eV and $\lambda = 0.318$ eV (κ_X , κ_A and λ are consistent with dimensionless normal coordinates).

The electronic states X and A of the butatriene cation were obtained at the MRCI/cc-pVTZ level of theory. First, ROHF orbitals were calculated, then state-averaged CASSCF(5,4) computations were carried out using equal weights for the two cationic states with 11 closed-shell orbitals and 4 active orbitals. The final step involved the internally-contracted MRCI method implemented in the Molpro program (version 2020.2). Permanent and transition dipole moments, needed to construct the Hamiltonian of Eq. (23), were obtained at several different nuclear configurations.

B. Diabatic representation of the permanent and transition dipole moment surfaces

As the system is described using the diabatic representation, we need to construct the diabatic PDM and TDM surfaces. This can be achieved by diagonalizing the diabatic potential energy matrix of Eq. (24) for each nuclear configuration,

$$\mathbf{U}^T \begin{bmatrix} V_X & V_{XA} \\ V_{XA} & V_A \end{bmatrix} \mathbf{U} = \begin{bmatrix} V_{\text{lower}} & 0 \\ 0 & V_{\text{upper}} \end{bmatrix} \quad (33)$$

which results in the transformation matrix \mathbf{U} and lower and upper adiabatic PESs (V_{lower} and V_{upper}). Since ab initio calculations presented in the previous subsection yield PDM and TDM surfaces in the adiabatic representation, the transformation

$$\begin{bmatrix} \mu_X & \mu_{XA} \\ \mu_{XA} & \mu_A \end{bmatrix} = \mathbf{U} \begin{bmatrix} \mu_X^{\text{ad}} & \mu_{XA}^{\text{ad}} \\ \mu_{XA}^{\text{ad}} & \mu_A^{\text{ad}} \end{bmatrix} \mathbf{U}^T \quad (34)$$

is invoked to construct the diabatic PDM (μ_X and μ_A) and TDM (μ_{XA}) surfaces.

As already discussed in Section I, the diabatic PDM and TDM surfaces can be approxi-

mated by first-order Taylor expansion about the FC point,

$$\begin{aligned}
\mu_X &= \left(\frac{\partial \mu_X}{\partial Q_{\text{PDM}}} \right) \Big|_{\text{FC}} Q_{\text{PDM}} = \beta_X Q_{\text{PDM}} \\
\mu_A &= \left(\frac{\partial \mu_A}{\partial Q_{\text{PDM}}} \right) \Big|_{\text{FC}} Q_{\text{PDM}} = \beta_A Q_{\text{PDM}} \\
\mu_{XA} &= \left(\frac{\partial \mu_{XA}}{\partial Q_{\text{TDM}}} \right) \Big|_{\text{FC}} Q_{\text{TDM}} = \gamma Q_{\text{TDM}}
\end{aligned} \tag{35}$$

where PDM and TDM derivatives can be estimated by the method of finite differences. Since \mathbf{U} equals the two-dimensional identity matrix in the close vicinity of the FC point, PDM and TDM derivatives in the adiabatic and diabatic representations coincide. Therefore, one can directly use dipole derivatives provided by ab initio calculations: $\beta_X = 1.05 \cdot 10^{-3}$ au, $\beta_A = -1.89 \cdot 10^{-3}$ au and $\gamma = -4.37 \cdot 10^{-4}$ au, given in atomic units.

V. ADDITIONAL FIGURES

Fig. 6 and Fig. 7 show 4-mode cavity-free (blue) and cavity (red) ionization spectra with $\omega_{\text{cav}} = 645.02 \text{ cm}^{-1}$ and $g = 0.15$ au, and $\omega_{\text{cav}} = 824.80 \text{ cm}^{-1}$ $g = 0.1$ au, respectively. In both cases, three panels of the figures correspond to the following three different cavity field polarizations (see Fig. 5 for the definition of body-fixed Cartesian axes): $\mathbf{e} = (0, 1, 0)$ (only PDMs), $\mathbf{e} = (1, 0, 0)$ (only TDM) and $\mathbf{e} = (1, 1, 0)/\sqrt{2}$ (both TDM and PDMs).

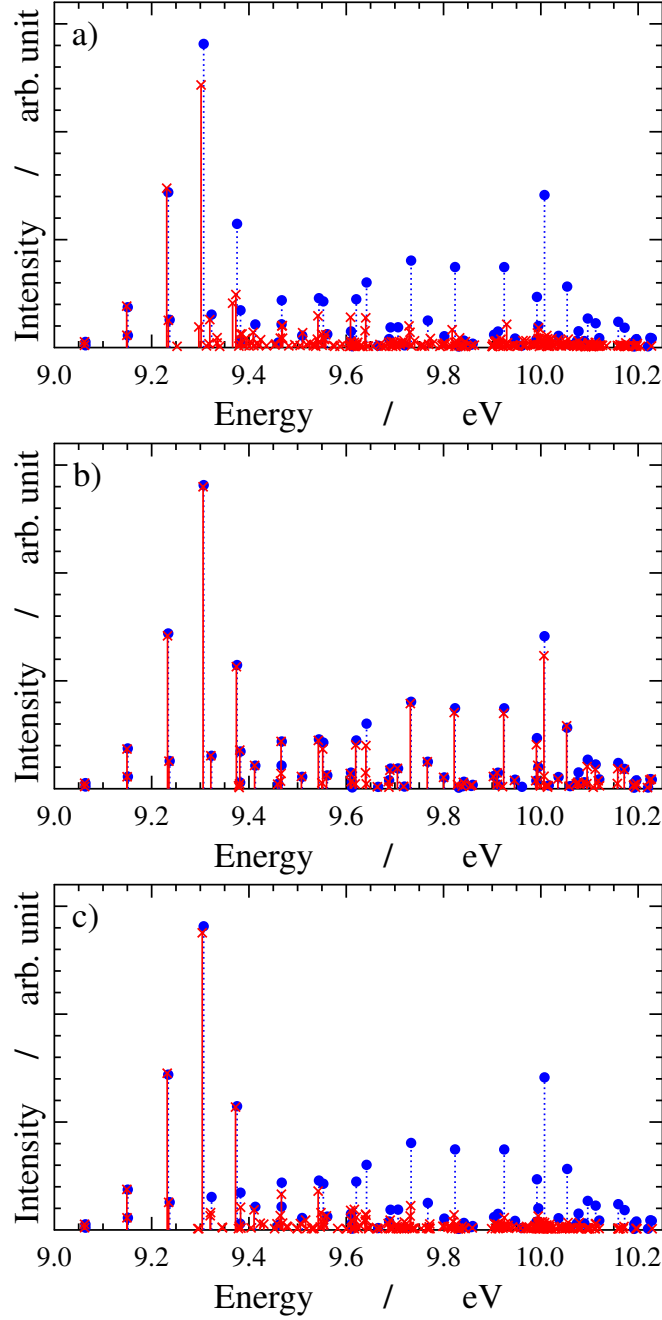


Figure 6. Cavity-free (blue) and cavity (red) ionization spectra of butatriene with cavity parameters $\omega_{\text{cav}} = 645.02 \text{ cm}^{-1}$ and $g = 0.15 \text{ au}$. The field polarization vector is chosen in three different ways: (a) $\mathbf{e} = (0, 1, 0)$ (only permanent dipole moments (PDMs)), (b) $\mathbf{e} = (1, 0, 0)$ (only transition dipole moment (TDM)), and (c) $\mathbf{e} = (1, 1, 0)/\sqrt{2}$ (both TDM and PDMs).

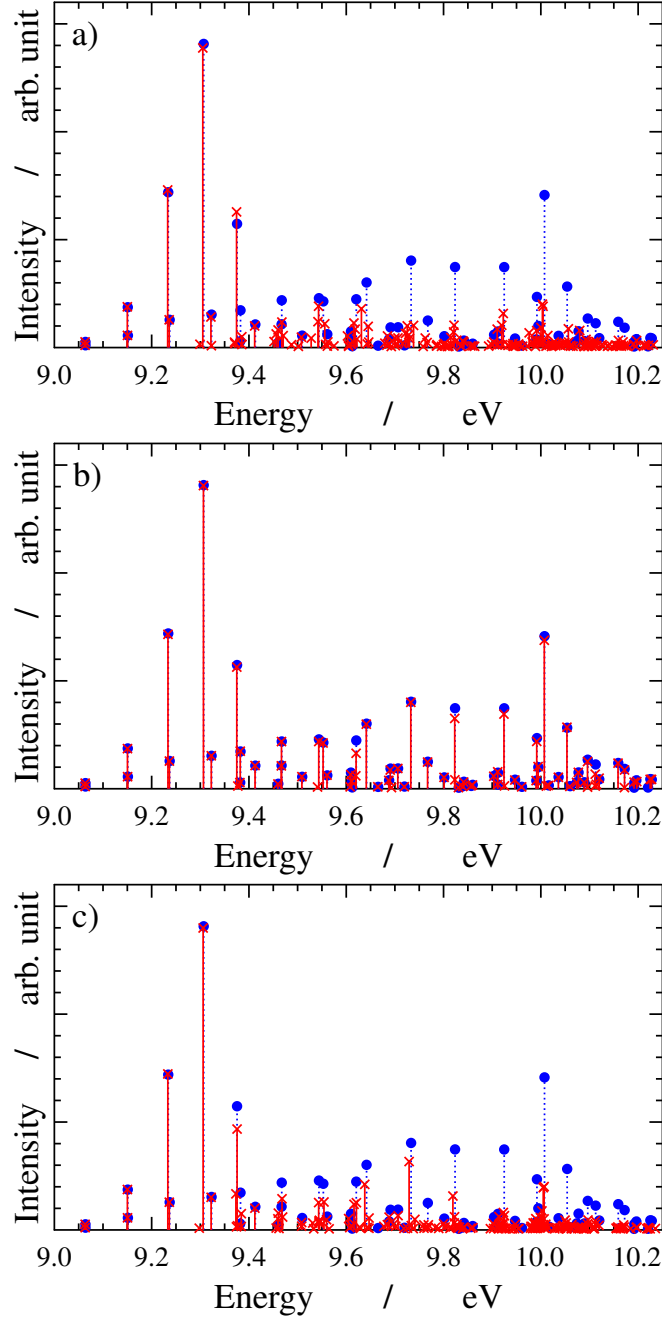


Figure 7. Cavity-free (blue) and cavity (red) ionization spectra of butatriene with cavity parameters $\omega_{\text{cav}} = 824.80 \text{ cm}^{-1}$ and $g = 0.1 \text{ au}$. The field polarization vector is chosen in three different ways: (a) $\mathbf{e} = (0, 1, 0)$ (only permanent dipole moments (PDMs)), (b) $\mathbf{e} = (1, 0, 0)$ (only transition dipole moment (TDM)), and (c) $\mathbf{e} = (1, 1, 0)/\sqrt{2}$ (both TDM and PDMs).